2014 American Control Conference (ACC)
June 4-6, 2014. Portland, Oregon, USA

Transient Losses in Synchronizing Renewable Energy Integrated Power Networks

Emma Sjödin and Dennice F. Gayme

Abstract— **This paper quantifies the transient power losses incurred in re-synchronizing a network of generators and loads. The power system is represented using a network preserving model with loads and asynchronous generators modeled as frequency dependent power injections, which we refer to as 'first-order oscillators'. Coupling these models with the swing equations of traditional generators leads to a mixed-oscillator system. The power flows used to maintain network synchronization induce resistive (real power) losses in the system, which we quantify through an $\mathcal{H}_2$ norm that is shown to scale with network size. Our results also show that given a fixed network size, this $\mathcal{H}_2$ norm is the same for first-order, second-order and mixed-oscillator systems, provided that the damping coefficients are all equal. Therefore, if the renewable power generators being added to a power network can be controlled so that their effective dampings match those of the existing generators, they will not increase transient power losses in the system.**

I. Introduction

Renewable energy is making up an increasing fraction of world-wide electricity production. This widespread growth is being driven by concerns about climate change, increasing fossil fuel prices [1], [2] and government mandates [3]. Energy grids of the future are expected to become increasingly distributed with numerous smaller, local generation resources replacing large centralized power plants [4]. Renewable energy integrated decentralized power grids are already becoming prevalent in the developing world because of lower initial investment costs [4]. The natural variability of solar and wind power is also expected to result in higher amplitude and more frequent power fluctuations [3], [5]. This increased variability may affect the system's ability to maintain synchronous operation and to regain synchrony after a disturbance [6], its so-called rotor angle or synchronous stability. Here we define synchrony as the condition when the frequencies of all generators within a particular power network are aligned and the phase angles are at a steady state operating condition, i.e., there are no angular swings in the system [6], [7]. There is a large body of related literature on power system stability, see e.g. [8] for a survey of early literature and [9] for more recent developments.

There has been limited research into the transient stability properties of renewable energy integrated power systems. Typical power system stability analysis is carried out using a Kron reduced network of generators. However, most renewable energy based power generation does not use synchronous generators, so a system of coupled swing equations cannot be used to analyze the stability of systems with substantial renewable energy penetration. Moreover, a canonical modeling paradigm that captures the dynamics of interest has yet to be established [10]–[12]. The Kron reduced network model also has questionable applicability to renewable energy integrated grids because it lacks a mechanism to represent loads and asynchronous generation, and does not preserve the network topology [7]. These aspects make it ill-suited to capture asynchronous generation or new phenomena such as demand-side energy control systems that rapidly shift loads to maintain power balance in the face of renewable energy source variability [5].

In this paper, we represent a renewable energy integrated power system using a network preserving model with loads and asynchronous generators represented as frequency dependent power injections. By abuse of terminology we refer to these power injection models as 'first-order oscillators.' The full system then consists of these first-order oscillator dynamics coupled with the classical machine model of synchronous generators. We refer to this system as a mixed-oscillator network or a system of first- and second-order oscillator dynamics. Coupled oscillator networks have been studied in a number of applications, such as biological networks, vehicle and robot consensus problems, see [13] for a survey. In the context of power systems stability, these mixed-oscillator dynamics were first proposed by Bergen and Hill [14] as a model that preserves the power system network structure while explicitly including loads.

We first show that the Bergen and Hill [14] load models can be trivially extended to represent the dynamics of both induction generators and the type of droop-controlled power inverters commonly used in solar and wind power plants. The mixed-oscillator model adopted here is appealing for studying synchronization dynamics because it captures the relationships between active power and frequency in terms of the same states as the classical machine model. A similar model was recently employed to characterize the rate of convergence (damping) in heterogenous power networks [15]. While the literature offers a number of more detailed descriptions of asynchronous machines, particularly wind turbine generators [16]–[18], it unclear how these models would be adapted to studies of rotor angle stability [19].

The modeling framework described above is used to quantify the resistive (real power) losses incurred in maintaining or regaining a synchronous state in a power system with variable renewable energy sources. In other words, rather than

E. Sjödin is with the Department of Mechanical Engineering at the Johns Hopkins University, Baltimore, MD, USA, 21218 and the School of Electrical Engineering, KTH Royal Institute of Technology, SE-100 44 Stockholm, Sweden. (emmsjo@kth.se)
D. F. Gayme is with the Department of Mechanical Engineering at the Johns Hopkins University. (dennice@jhu.edu)

978-1-4799-3274-0/$31.00 ©2014 AACC

characterize the stability of the system, we instead evaluate the control signal, in terms of real power losses, required to achieve this synchrony. The analysis thus assumes that all disturbances are sufficiently small to allow the study of the linearized system. We model the mixed-oscillator dynamics as a linear system subject to distributed disturbances and define the system output such that the squared $\mathcal{H}_2$ norm quantifies the resistive power losses. We then verify that the resulting system is asymptotically stable.

Our main result shows that given a fixed network size, systems of first-order, second-order and mixed-oscillators have the same transient power losses, provided their damping coefficients are equal. This result is striking considering the fundamental differences in the transient behavior of these three types of systems, in fact the so-called 'first-order oscillators' are not actually oscillators. It also has interesting implications for power grids of the future, which are expected to have more renewable energy sources and to be increasingly distributed. In particular, our main result indicates that the expected increase in transient losses associated with adding renewable power sources can be eliminated if the power electronics of the new renewable power plant can be adjusted so that its damping matches that of the existing synchronous generators. Transient resistive power losses have previously been shown to scale linearly with the network size and their importance is thus expected to increase as generation becomes more distributed [20].

The remainder of this paper is organized as follows. In Section II, we introduce the system model and justify the use of the first-order model to capture renewable power systems. In Section III, we first show that the input-output linear system is stable and evaluate its $\mathcal{H}_2$ norm. We then draw comparisons between our main findings and previous results. We illustrate the theory in the case study of Section IV and conclude in Section V.

II. Problem Formulation

Consider a network with a set of nodes (buses) $\mathcal{V} := \{1, \dots n_0\}$ connected by a set $\mathcal{E}_0$ of edges (lines). Each node $i \in \mathcal{V}$ contains a frequency dependent element (either a frequency-dependent load or asynchronous power source) and $m \leq n_0$ of these buses make up the subset of synchronous generator nodes $\mathcal{G} \subset \mathcal{V}$.

The network preserving model is derived by augmenting the network as follows. Divide each generator bus $j \in \mathcal{G}$ into two separate buses; one containing the synchronous generator and one with a frequency dependent element. Then connect the resulting two-bus subsystem with a purely reactive line. This line represents the transient reactance of the synchronous generator. The system is then described by an augmented network with $n = n_0 + m$ nodes. We refer to the m synchronous generators nodes in this augmented network as 'fictitious generator buses'. Fig. 1 illustrates this procedure for a 5 bus network.

Each node in the augmented n-bus network has voltage magnitude $|V_i|$ and voltage phase angle θ_i. Without loss of generality the buses can be renumbered such that the buses without synchronous generation in the original network are nodes $\{1, ..., n_0 - m\} =: \mathcal{W}$, the synchronous (fictitious) generator buses are nodes $\{n_0 + 1, ..., n_0 + m = n\} =: \mathcal{G}_1$ and the new buses (i.e. the frequency-dependent elements in the new two-node subsystems), are nodes $\{n_0 - m + 1, ..., n_0\} =: \mathcal{L}$. The nodes $i \in \mathcal{L}$ are numbered in increasing order with respect to $\mathcal{G}$. Furthermore, we denote the set of the m lossless lines used to augment the system as $\mathcal{E}_{\text{aug}}$. The full sets of nodes and edges in the augmented system are then respectively denoted $\mathcal{N} := \mathcal{W} \cup \mathcal{G}_1 \cup \mathcal{L}$ and $\mathcal{E} = \mathcal{E}_0 \cup \mathcal{E}_{\text{aug}}$.

Remark 1: The system augmentation method outlined above and the analysis throughout this paper assume that each node $i \in \mathcal{G}$ has a frequency dependent element (i.e. a non-zero load or frequency dependent power source is co-located with every synchronous generator in the pre-augmented system). The augmentation method and analysis can easily be adapted to include isolated synchronous generators. In the augmentation, these nodes remain single synchronous generator buses with the transient reactance of the generator captured in the surrounding transmission lines.

A. Model of Loads and Asynchronous Machines

We now introduce the frequency-dependent load and asynchronous machine models that are adapted from the framework in [14]. We model the power load drawn from each bus $i \in \mathcal{L}$ as

$$P_{\text{load},i} = P^0_{\text{load},i} + D_i \omega_i, \tag{1}$$

where $P^0_{\text{load},i}$ is the constant steady-state power drawn, $D_i > 0$ is the frequency coefficient for each load and $\omega_i = \dot{\theta}_i$ is the corresponding frequency.

The model (1) was originally proposed in [14] as a dynamical representation of real power loads and has since been used to represent induction motors drawing power from the grid [19]. It captures the relationship between the active power and frequency in induction machines by modeling it as a linear function of the slip, i.e., the difference between the rotational speed of machine and the grid. Since induction generators, such as fixed-speed wind turbines with cage-type generators, work in the same way as induction motors, equation (1) is also a suitable model for asynchronous generators. We thus model asynchronous machines at each bus $i \in \mathcal{W}$ as frequency-dependent power injections of the form

$$P_{\text{wind},i} = P^0_{\text{wind},i} - D_i \omega_i, \tag{2}$$

where $P^0_{\text{wind},i}$ is the constant steady-state input, $D_i > 0$ is the frequency coefficient for each generator and the we use the index "wind" to refer to renewable power generation. These power injections differ from the loads in that they enter the bus power balance with a positive sign to signify that they are injecting power to the system. The magnitude of the parameters D_i also tend to be different for loads versus renewable generation systems.

The frequency-dependent power injection model (2) is also applicable to the increasingly common variable speed wind farm generators and other renewable power sources such as

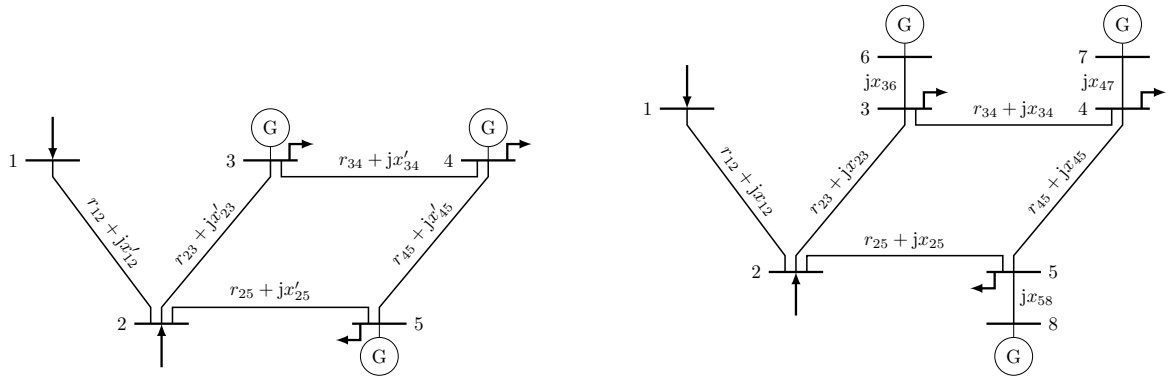

(a) Original network (b) Augmented network

Fig. 1: An example of (a) a 5 bus network with 3 generators and (b) the corresponding augmented network, in which every generator/load bus is replaced by a load bus and a fictitious generator bus and the nodes are relabeled such that $\mathcal{W} = \{1, 2\}$, $\mathcal{G}_1 = \{6, 7, 8\}$ and $\mathcal{L} = \{3, 4, 5\}$. The lines in $\mathcal{E}_{\text{aug}} = \{\mathcal{E}_{36},\ \mathcal{E}_{47},\ \mathcal{E}_{58}\}$ are the purely reactive lines that model the transient reactances of the generators, which in (a) are absorbed into x'_{ij}. The arrows at buses 1 and 2 symbolize a power injection by an asynchronous generation source.

photovoltaics. These devices require DC/AC power converters (inverters) and associated controlled power electronics to interface with the grid. One algorithm that is commonly employed in the converter is the following droop control law, which aims to regulate the frequency such that the system emulates the behavior of a synchronous machine.

$$\omega_i = \omega^* - k_i(P_{e,i} - P_i^*), \tag{3}$$

where $P_{e,i}$ is the active power demand at bus i and P_i^* is the constant power injected to the grid when operated at the rated frequency ω^*. k_i is the so-called droop coefficient. Simpson-Porco et al. [21] show that there is an exact correspondence between the droop control law (3) and our proposed model (2). Therefore, we conclude that (2) is well-suited to capture the physics of several types of renewable generation in power systems. Furthermore, since (2) is in terms of the same states as the classical machine model it is well suited to synchronous stability studies. It is unclear how more detailed models that include current, voltage and other parameters internal to the machine structure can be applied to transient stability analysis for the overall power system [19].

B. System Dynamics

The swing equation for the synchronous generators is

$$M_i\ddot{\theta} + \beta_i\dot{\theta} = P^0_{m,i} - P_{e,i}, \tag{4}$$

where M_i and β_i are respectively the inertia and damping coefficient of the i^{th} generator, and $P^0_{m,i}$ is the constant mechanical power input from the generator turbine. For all buses $i \in \mathcal{N}$, $P_{e,i}$ is the electrical power input to the grid. Combining the swing equations with (1) and (2) leads to following dynamics at each node $i \in \mathcal{N}$

$$M_i\ddot{\theta}_i + \beta_i\dot{\theta}_i + D_i\dot{\theta}_i = P^0_{m,i} + P^0_{\text{wind},i} - P^0_{\text{load},i} - P_{e,i},$$

where $D_i = 0$, $M_i > 0$, $\beta_i > 0$ and $P^0_{m,i} > 0$ for $i \in \mathcal{G}_1$; $M_i = \beta_i = 0$, $D_i > 0$ and $P^0_{\text{wind},i} > 0$ for $i \in \mathcal{W}$; and $M_i = \beta_i = 0$, $D_i > 0$ and $P^0_{\text{load},i} > 0$ for $i \in \mathcal{L}$.

The real electrical power injected to the grid at node i is given by

$$\begin{aligned} P_{e,i} \;=\; & \bar{g}_i|V_i|^2 + \sum_{j\sim i} g_{ij}|V_i|\,|V_j|\cos(\theta_i - \theta_j) \\ & + \sum_{j\sim i} b_{ij}|V_i|\,|V_j|\sin(\theta_i - \theta_j), \end{aligned} \tag{5}$$

where $j \sim i$ denotes a line (edge) $\mathcal{E}_{ij} \in \mathcal{E}$, g_{ij} and b_{ij} are respectively the conductance and susceptance of that line, and $\bar{g}_i$ is the shunt conductance at bus i. Applying standard linear power flow assumptions, i.e., lossless lines, flat voltage profiles with $|V_i| = |V_0| = 1$ p.u. and small angle differences between adjacent nodes, to (5) yields

$$P_{e,i} = \sum_{j\sim i} b_{ij}(\theta_i - \theta_j). \tag{6}$$

To simplify the remaining notation, we define the bus admittance matrix $Y \in \mathbb{C}^{n\times n}$ as

$$Y_{ij} := \begin{cases} \bar{g}_i + \sum_{k\sim i}(g_{ik} - \mathbf{j}b_{ik}), & \text{if } i = j, \\ -(g_{ij} - \mathbf{j}b_{ij}), & \text{if } i \neq j \text{ and } j \sim i. \\ 0 & \text{otherwise.} \end{cases}$$

This admittance matrix can be decomposed into real and imaginary parts such that $Y = (L_G + \bar{G}) - \mathbf{j}L_B$, L_G denotes the matrix of conductances and L_B denotes the matrix of susceptances and $\overline{G} = diag\{\overline{g_i}\}$ denotes the matrix of shunt conductances. Both L_G and L_B define weighted graph Laplacians for the augmented network. In order to eliminate the inherent singularity of the graph Laplacians we define the reduced, or grounded, Laplacians $\tilde{L}_G$ and $\tilde{L}_B$, which are obtained by deleting the row and column corresponding to the grounded node as described in [22], [23]. For all of the analysis herein we will ground node n, which means that we set $\theta_n \equiv 0$ and measure all other phase angles and frequency deviations in the system with respect to this reference. This grounding allows node n to behave as an infinite bus.

In order to rewrite the dynamics in state space form we first define $\mathcal{M} = \mathrm{diag}\{M_i\}$, $\mathcal{B} = \mathrm{diag}\{\beta_i\}$ for buses $i \in \mathcal{G}_1$ and $D = \mathrm{diag}\{D_j\}$ for buses $j \in \mathcal{W} \cup \mathcal{L}$. We then write the dynamics of the load and asynchronous machine nodes ($j \in \mathcal{W} \cup \mathcal{L}$) and the synchronous generator nodes ($i \in \mathcal{G}_1$) respectively as

$$D\omega_D = -\begin{bmatrix} I_{n_0} & 0 \end{bmatrix} (\tilde{L}_B\theta - P^0) \quad (7)$$

$$\mathcal{M}\dot{\omega}_G + \mathcal{B}\omega_G = -\begin{bmatrix} 0 & I_{m-1} \end{bmatrix} (\tilde{L}_B\theta - P^0), \quad (8)$$

where $P^0 = \mathrm{diag}\{P_i^0\}$ and $P_i^0 = P_{m,i}^0 + P_{\mathrm{wind},i}^0 - P_{\mathrm{load},i}^0$. The state vectors are defined such that $\theta = \begin{bmatrix} \theta_1 & \cdots & \theta_{n-1} \end{bmatrix}^T$ and

$$\dot{\theta} = \begin{bmatrix} I_{n_0} \\ 0 \end{bmatrix} \omega_D + \begin{bmatrix} 0 \\ I_{m-1} \end{bmatrix} \omega_G = T_1\omega_D + T_2\omega_G. \quad (9)$$

Filling (7) into (9) allows the state ω_D to be eliminated using

$$T_1\omega_D = -T_1D^{-1}T_1^T(\tilde{L}_B\theta - P^0).$$

To simplify the notation, we define $T_D := T_1D^{-1}T_1^T$ and write the state equations the combined system as

$$\frac{\mathrm{d}}{\mathrm{d}t}\begin{bmatrix} \theta \\ \omega_G \end{bmatrix} = \begin{bmatrix} -T_D\tilde{L}_B & T_2 \\ -\mathcal{M}^{-1}T_2^T\tilde{L}_B & -\mathcal{M}^{-1}\mathcal{B} \end{bmatrix} \begin{bmatrix} \theta \\ \omega_G \end{bmatrix} + \begin{bmatrix} T_D \\ \mathcal{M}^{-1}T_2^T \end{bmatrix} \mathrm{w}. \quad (10)$$

Here we have lumped the constant power P^0 into the disturbance input w. In what follows, we will by some abuse of notation let the system (10) represent deviations from a steady-state operating point.

C. Transient Power Losses

When a balanced power system at a steady state operating point is subjected to disturbances re-synchronization is achieved through power flows that compensate for phase angle and frequency differences at adjacent nodes (relative to the nominal values of the balanced state operating point) [24]. These power flows during the synchronization transient lead to resistive power losses, which can be regarded as the control signal that drives the system back to a synchronous state. The real power flow over an edge $\mathcal{E}_{ij}$ is $P_{ij} = g_{ij}\left|V_i - V_j\right|^2$. Since we are regarding θ_i as the deviation from bus i's operating point, this power is equivalent to the resistive power loss over an edge during the transient. Simplifying this expression again using standard linear power flow assumptions along with trigonometric identities, leads to the following approximation these transient real power losses across the network.

$$\mathbf{P}_{\mathrm{loss}} = \sum_{i\sim j} g_{ij}|\theta_i - \theta_j|^2, \quad (11)$$

which is equivalent to the quadratic form $\mathbf{P}_{\mathrm{loss}} = \theta^*\tilde{L}_G\theta$. We can therefore define the $(n-1)$-dimensional output of the system (10) as

$$y = \begin{bmatrix} \tilde{L}_G^{1/2} & 0 \end{bmatrix} \begin{bmatrix} \theta \\ \omega_G \end{bmatrix}, \quad (12)$$

so that $\mathbf{P}_{\mathrm{loss}} = y^*y$. Since $\tilde{L}_G$ is a positive semi-definite graph Laplacian, we can take $\tilde{L}_G^{1/2}$ as its unique positive semi-definite matrix square-root. Note that no real power flows over the purely reactive lines that connect the two-node subsystems of the augmented network.

We can now define the system (10) and (12) as the input-output mapping H from w to y as

$$\frac{\mathrm{d}}{\mathrm{d}t}\begin{bmatrix} \theta \\ \omega_G \end{bmatrix} = \begin{bmatrix} -T_D\tilde{L}_B & T_2 \\ -\mathcal{M}^{-1}T_2^T\tilde{L}_B & -\mathcal{M}^{-1}\mathcal{B} \end{bmatrix} \begin{bmatrix} \theta \\ \omega_G \end{bmatrix} + \begin{bmatrix} T_D \\ \mathcal{M}^{-1}T_2^T \end{bmatrix} \mathrm{w} =: A\psi + B\mathrm{w} \quad (13a)$$

$$y = \begin{bmatrix} \tilde{L}_G^{1/2} & 0 \end{bmatrix} \begin{bmatrix} \theta \\ \omega_G \end{bmatrix} =: C\psi, \quad (13b)$$

where $\psi = [\theta, \omega_G]^T$.

We are interested in the resistive losses incurred during the transient period over which the system recovers synchrony after a disturbance, which can be obtained as the squared $\mathcal{H}_2$ norm of the system (13). The use of this $\mathcal{H}_2$ norm to quantify the transient power losses is motivated by some of the norm's standard interpretations, which include: *(a)* The variance of the output y when the disturbance input w is a unit variance white noise; *(b)* The total time integral of the variance of y when the initial condition is a random variable with correlation matrix BB^*; and *(c)* The sum of time integrals over output responses given an impulse disturbance input at each generator. The reader is referred to [20] for a more detailed discussion of the interpretation of this norm in terms of transient power losses.

III. Input-Output Analysis

In this section, we first show that the linear system (13) is asymptotically stable in order to ensure that its $\mathcal{H}_2$ norm exists. We then derive an expression for this norm and discuss upper and lower bounds on its value. Following that, we relate this norm to previous results on systems of first- and second-order oscillators. We end the section with a discussion of the implications of these results.

A. Stability

We show asymptotic stability of the system using the following lemma, whose proof follows the arguments in [14].

Lemma 3.1: The system (13) is asymptotically stable and the following is a Lyapunov function for (13a)

$$V(\theta, \omega_G) = \tfrac{1}{2}\theta^T\tilde{L}_B\theta + \tfrac{1}{2}\omega_G^T\mathcal{M}\omega_G.$$

Proof: Clearly, $V(0,0) = 0$. $\mathcal{M} > 0$ by definition and $\tilde{L}_B$ is positive definite, since it is a reduced Laplacian of a complete graph, see e.g. [25]. Therefore, $V(\theta, \omega_G) > 0, \ \forall\theta, \omega_G \neq (0,0)$. The derivative of V evaluated along the state trajectories is, after some algebraic operations, given by

$$\dot{V}(\theta, \omega_G) = -\omega_G^T\mathcal{B}\omega_G - \theta^T\tilde{L}_BT_D^T\tilde{L}_B\theta$$

which is non-positive for all θ, ω_G, since $\mathcal{B} > 0$ and $\tilde{L}_BT_D^T\tilde{L}_B \geq 0$. For asymptotic stability, we also require $\dot{V}(\theta, \omega_G) \equiv 0 \ \Leftrightarrow \ (\theta, \omega_G) \equiv (0,0)$. Clearly, $\dot{V} \equiv 0$

requires $\omega_G \equiv 0$ and $T_D^T \tilde{L}_B \theta \equiv 0$. The latter is equivalent to $T_1^T \tilde{L}_B \theta \equiv 0$. By (10), however, $\omega_G \equiv 0$ implies $-\mathcal{M}^{-1} T_2^T \tilde{L}_B \theta \equiv 0$. Now, if $T = \begin{bmatrix} T_1 & T_2 \end{bmatrix} = I_{n_0+m-1}$, the two give $T\tilde{L}_B\theta \equiv 0$. Since T is the identity matrix and $\tilde{L}_B$ is positive definite, $\theta \equiv 0$. We therefore conclude that the last criterion holds and all Lyapunov's conditions for global asymptotic stability are fulfilled. ■

B. $\mathcal{H}_2$ Norm Calculations

The $\mathcal{H}_2$ norm of the system H in (13) can be computed as

$$||H||_{\mathcal{H}_2}^2 = \mathrm{tr}(B^* X B), \tag{14}$$

where X is the observability Gramian given by the Lyapunov equation $A^*X + XA = -C^*C$. If we partition $X \in \mathbb{C}^{(n+m-2)\times(n+m-2)}$ into four submatrices as

$$X = \begin{bmatrix} X^{11} & X^0 \\ X^{0*} & X^{22} \end{bmatrix},$$

where $X^{11} \in \mathbb{C}^{(n-1)\times(n-1)}$, $X^0 \in \mathbb{C}^{(n-1)\times(m-1)}$ and $X^{22} \in \mathbb{C}^{(m-1)\times(m-1)}$, this Lyapunov equation reduces to the following three linearly independent equations

$$\tilde{L}_B T_D X^{11} + \tilde{L}_B T_2 \mathcal{M}^{-1} X^{0*} + X^{11} T_D \tilde{L}_B + X^0 \mathcal{M}^{-1} T_2^T \tilde{L}_B = \tilde{L}_G \tag{15a}$$

$$\tilde{L}_B T_D X^0 - \tilde{L}_B T_2 \mathcal{M}^{-1} X^{22} + X^{11} T_2 - X^0 \mathcal{M}^{-1} \mathcal{B} = 0 \tag{15b}$$

$$T_2^T X^0 - \mathcal{M}^{-1} \mathcal{B} X^{22} + X^{0*} T_2 - X^{22} \mathcal{M}^{-1} \mathcal{B} = 0. \tag{15c}$$

Using these expressions (14) becomes

$$||H||_{\mathcal{H}_2}^2 = \mathrm{tr}(T_D^2 X^{11}) + \mathrm{tr}(\mathcal{M}^{-2} X^{22}). \tag{16}$$

Assuming uniform dampings and inertia, i.e. $D = \bar{D} I_{n_0}$, $\mathcal{B} = \beta I_{m-1}$ and $\mathcal{M} = M I_{m-1}$, (16) can be simplified to:

$$||H||_{\mathcal{H}_2}^2 = \frac{1}{2\bar{D}} \mathrm{tr}(\tilde{L}_B^{-1} \tilde{L}_G) + \left(1 - \frac{\beta}{\bar{D}}\right) \frac{1}{M^2} \mathrm{tr}(X^{22}), \tag{17}$$

where X^{22} can be evaluated using equations (15a)-(15c).

C. Generalized Laplacian Ratios

In order to understand the losses described in the expression (17), it is useful to first examine the properties of $\mathrm{tr}(\tilde{L}_B^{-1} \tilde{L}_G)$, i.e. the first term in the expression (17), which we term the generalized graph Laplacian ratio. In order to facilitate this discussion we restate a Lemma from [22], which is required to prove this paper's main result.

Lemma 3.2: Given a grounded node n. Let $\tilde{L}_G$ and $\tilde{L}_B$ be the reduced, or grounded, Laplacians obtained by deleting the n^{th} rows and columns of the two weighted graph Laplacians L_G and L_B defined in Section II-B. Then

$$\mathrm{tr}(\tilde{L}_B^{-1} \tilde{L}_G) = \mathrm{tr}(L_B^\dagger L_G), \tag{18}$$

where † denotes the Moore-Penrose pseudo inverse.

Proof: The reader is referred to [22] for a proof for the special case of the Kron reduced network. The difference for the augmented network discussed herein is as follows. The graph underlying L_B for the augmented system defined in Section II-B is connected and $\tilde{L}_B$ is non-singular, while the weighted graph for L_G is not connected and $\tilde{L}_G$ has m zero eigenvalues. However, both L_B and L_G are weighted graph Laplacians for the augmented system and the proof in [22] only requires that L_G is a graph Laplacian. Therefore, the lemma in [22] extends to the augmented system. ■

The notion that $\mathrm{tr}(\tilde{L}_B^{-1} \tilde{L}_G)$ is a generalized ratio between the conductance and susceptance matrices is further strengthened by the following result, which shows that for our augmented network, the purely reactive edges (connected to the fictitious generator buses in the set $\mathcal{G}_1$) do not contribute to the generalized Laplacian ratio. In other words, the augmented, fictitious nodes are irrelevant and only the main network, connecting nodes $j \in \{1, \ldots, n_0\} =: \mathcal{L} \cup \mathcal{W}$, influence $\mathrm{tr}(\tilde{L}_B^{-1} \tilde{L}_G)$. This idea is formalized through the following theorem.

Theorem 3.3: Consider a network (graph) of n_0 nodes connected by the set $\mathcal{E}_0 = \{\mathcal{E}_{ij}\}$ of edges with weights $b_{ij} > 0$ and $g_{ij} > 0$ respectively. Denote the weighted graph Laplacians associated with each of these weights as L_B^0 and L_G^0 respectively.

Then, following the procedure illustrated for the power network in Fig. 1, divide $m \leq n_0$ of these nodes each into two nodes to create m new augmented nodes (e.g. construct the set $\mathcal{G}_1$ in Section II). Denote the edges connecting these augmented nodes $\mathcal{E}_{\mathrm{aug}}$ and set the associated edge weights such that $b_{ij} > 0$ and $g_{ij} = 0$ for each $\mathcal{E}_{ij} \in \mathcal{E}_{\mathrm{aug}}$. Then denote the graph Laplacians associated with edge weights b_{ij} and g_{ij} for $\mathcal{E}_{ij} \in \mathcal{E} := \mathcal{E}_0 \cup \mathcal{E}_{\mathrm{aug}}$ of the full augmented network with $n_0 + m = n$ nodes as L_B and L_G respectively. If their grounded versions, with the n^{th} rows and columns deleted are given by $\tilde{L}_B$ and $\tilde{L}_G$, then

$$\mathrm{tr}(\tilde{L}_B^{-1} \tilde{L}_G) = \mathrm{tr}(L_B^\dagger L_G) = \mathrm{tr}(L_B^{0\dagger} L_G^0).$$

Proof: See [26] for the proof. ■

The fact that only the main, unaugmented, network affects the generalized Laplacian ratio can be more clearly seen when the conductance to susceptance ratios of all lines (edges) are equal. The following corollary shows that for this special case, the generalized Laplacian ratio scales directly with the number of nodes in the non-augmented system.

Corollary 3.4: Consider the network described in Theorem 3.3. Let the edges $\mathcal{E}_{ij} \in \mathcal{E}_0$ have equal resistance to reactance ratios, i.e., $\alpha_{ij} = \frac{r_{ij}}{x_{ij}} = \frac{g_{ij}}{b_{ij}} = \alpha$. Then

$$\mathrm{tr}(\tilde{L}_B^{-1} \tilde{L}_G) = \alpha(n_0 - 1). \tag{19}$$

Proof: In this case, $L_G^0 = \alpha L_B^0$. By Theorem 3.3 and Lemma 3.2: $\mathrm{tr}(\tilde{L}_B^{-1} \tilde{L}_G) = \mathrm{tr}(L_B^{0\dagger} L_G^0) = \mathrm{tr}((\tilde{L}_B^0)^{-1} \tilde{L}_G^0) = \mathrm{tr}((\tilde{L}_B^0)^{-1} \alpha \tilde{L}_B^0) = \mathrm{tr}(\alpha I_{n_0-1}) = \alpha(n_0 - 1)$. ■

Remark 2: Note that Theorem 3.3 and Corollary 3.4 allow for the edges $\mathcal{E}_{ij} \in \mathcal{E}_{\mathrm{aug}}$ to have any non-zero reactance x_{ij}.

D. Relation to Previous Results

From (16) it is clear that when $\beta = \bar{D}$, the $\mathcal{H}_2$ norm of the system H reduces to

$$||H||_{\mathcal{H}_2}^2 = \frac{1}{2\bar{D}} \mathrm{tr}(\tilde{L}_B^{-1} \tilde{L}_G). \tag{20}$$

The frequency dependence coefficient D in (1) and (2) characterizing the asynchronous generators and power loads

can be interpreted as a type of damping, analogous to the dampings β of the synchronous generators. However, wind power plants and loads generally have less inertia than traditional synchronous generators. It is thus reasonable to assume $\beta \geq D$, which leads to the following upper bound on (16)

$$||H||^2_{\mathcal{H}_2} \leq \frac{1}{2\bar{D}} \mathrm{tr}(\tilde{L}_B^{-1} \tilde{L}_G). \tag{21}$$

Even in the general case of non-uniform asynchronous dampings, a choice of $\bar{D} = \min_{i=1,\dots,n_0} D_i = D_{\min}$ makes this bound conservative.

An interesting special case occurs if $m = 0$, which corresponds to a network of first-order oscillators, i.e., a system without synchronous generation in our modeling framework. The resulting model, which is a linear version of the Kuramoto oscillator model, is relevant for ongoing research on renewable energy dominated power systems. For instance, the authors of [21] show that the (nonlinear) Kuramoto model is an exact representation of droop-controlled inverters in a microgrid, e.g. a system with distributed renewable generation in a low-voltage network.

In order to study this model, we let L_B^0 and L_G^0 be the susceptance and conductance matrices (or weighted graph Laplacians) for this network of n_0 nodes. In this case, we can no longer ground a synchronous generator node and must instead choose a node $k \in \mathcal{L} \cup \mathcal{W}$ as the reference. We respectively denote the corresponding grounded susceptance and conductance matrices as $\tilde{L}_B^0$ and $\tilde{L}_G^0$. If we assume that all of nodes have the same damping coefficient $D_i = \bar{D}$ for all $i \in \mathcal{L} \cup \mathcal{W}$, we can then write the input-output mapping $\tilde{H}_{1^{st}}$ for the first-order dynamical system as

$$\begin{aligned} \frac{\mathrm{d}}{\mathrm{d}t}\tilde{\theta} &= -\frac{1}{\bar{D}}\tilde{L}_B^0\tilde{\theta} + \frac{1}{\bar{D}} I\tilde{\mathrm{w}} \\ \tilde{y} &= (\tilde{L}_G^0)^{1/2}\tilde{\theta}, \end{aligned} \tag{22}$$

where $\tilde{\theta}$ is the state vector of the $n_0 - 1$ bus angles of the reduced system. It is then easy to show that $||\tilde{H}_{1^{st}}||^2_{\mathcal{H}_2} = \frac{1}{2\bar{D}}\mathrm{tr}((\tilde{L}_B^0)^{-1}\tilde{L}_G^0)$, which by Lemma 3.2 and Theorem 3.3 is equivalent to (20).

By considering $\bar{D}$ to be a surrogate for the damping coefficient β, and provided the network remains unchanged, (20) is also the norm of a system with n_0 second-order oscillators [22], [27]. In addition, the system (13) reduces to the second-order model if $n_0 = m$ and the system is not augmented, see Remark 1. The main result of this section shows that this $\mathcal{H}_2$ norm is also that of a network of n_0 first-order oscillators with dampings $\bar{D}$, augmented with m second-order oscillators with dampings $\beta = \bar{D}$. I.e., the m additional nodes, which change the overall system dynamics but do not change the norm.

We can conclude that if the uniform damping parameters are used, the $\mathcal{H}_2$ norm and therefore the resistive losses are the same, regardless of whether the first-order (22), a second-order or the combined model (13) is used. Any differences in the resistive losses thus depend on the parameters that describe the different types of generators. These differences, as well as any loss-related synergies arising in the combined model due to coupling of the parameters, are explored in the case study in Section IV.

We should point out that these results do not claim the models to be equivalent, and do not address power system transient stability properties. The transient responses of the respective systems are substantially different and for a stability analysis, the model order and parameters should be chosen with care. The losses incurred in a synchronizing network and the network's ability to synchronize are two different issues, and it is only in terms of the $\mathcal{H}_2$ norm of the system described in (13a) with output (13b) that the different order models are equivalent.

Remark 3: System (22) assumes a system in which one node is grounded. We point out that the grounded system's $\mathcal{H}_2$ norm is equivalent to that of a full system [22]. The same result holds for H in (13) if $\beta_i = D_i = \bar{D} \ \ \forall i \in \mathcal{N}$.

IV. Case Study

The result (17) indicates that the transient real power losses in a network of coupled first- and second-order oscillators primarily depends on its sub-network of first-order oscillators with damping coefficients $\bar{D}$. The influence of the second-order oscillators, the synchronous generators, increases as the damping coefficient β increases. In this section, we present a brief case study using in the network depicted in Figure 1b to illustrate how these losses scale with the damping and internal transient reactance of each synchronous machine.

To simplify the discussion, we consider a system with equal impedances $z_{ij} = 0.05 + \mathbf{j}0.25$ for all edges $\mathcal{E}_{ij} \in \mathcal{E}_0$. Similarly, we let all asynchronous machines have the same frequency coefficient $\bar{D} = \frac{5}{2\pi f_0}$, where $f_0 = 60$ Hz. We set the inertia for all three synchronous generators to $M = \frac{20}{2\pi f_0}$ and vary their common damping β as multiples of the asynchronous damping D. Figure 2 shows how changes in β affect the transient losses in the network for a system with the following three different values of synchronous generator transient reactance, $x_{ij} \in \{0.01,\ 0.05,\ 0.1\}$ for $\mathcal{E}_{ij} \in \mathcal{E}_{\mathrm{aug}}$.

We note that while larger synchronous dampings reduce the synchronization losses of the system, the marginal effect of an increased damping decreases. The example indicates that, in accordance with the bound (21), it is the size of the asynchronous dampings that drives the size of the losses. The losses also depend on the transient reactances, where a smaller reactance implies smaller losses. An intuitive explanation for this is that a larger susceptance allows for more power to flow, which lets the larger damping of the synchronous generator attenuate more of the remaining system's oscillations. Note that the transient reactances are however irrelevant when $\beta = \bar{D}$. The losses are then given by (19), which we can compute as $||H||^2_{\mathcal{H}_2} = \frac{\alpha}{2\bar{D}}(n_0 - 1) = \frac{0.2}{2\cdot\frac{5}{2\pi 60}} \cdot 4 = 30.16$ for the parameters given in this example.

V. Conclusions

In this paper, we propose a network preserving model to capture the dynamics of renewable energy integrated power systems with loads and asynchronous generators represented

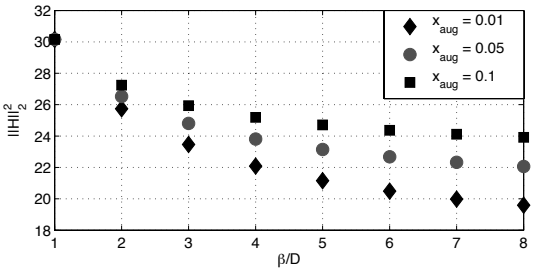

Fig. 2: The (squared) $\mathcal{H}_2$ norm (17) for the system depicted in Figure 1b with increasingly large synchronous generator dampings given three different synchronous generator transient reactances x_{aug}.

as frequency dependent power injections. The full system is then a mixed-oscillator system consisting of these so-called first-order oscillator dynamics and the second-order oscillators (swing equations), which model the synchronous generators. We then apply distributed disturbances to the network and quantify the transient resistive (real) power losses incurred in regaining or maintaining a synchronous state as the squared $\mathcal{H}_2$ norm of the system. Previous studies have shown that for Kron reduced synchronous generator networks, these transient power losses are independent of the network connectivity. Here we show that this result extends to the mixed-oscillator networks discussed here. We further show that, given a fixed network size, adding new loads and asynchronous generators (i.e., at an existing node) do not affect these transient losses, provided that the damping coefficients at all nodes are uniform. These results indicate that although renewable, asynchronous generators will alter the power system dynamics, they will not necessarily increase the transient power losses, if their dampings can be adjusted to match the existing synchronous generators. Since controlled power inverters are required for grid-integration of many renewable sources, the damping is often a design parameter. Therefore, these asynchronous machines can even be used to improve the overall system damping and to decrease transient power losses.

VI. Acknowledgements

The authors would like to thank Henrik Sandberg of KTH Royal Institute of Technology for his insightful comments and a number of interesting discussions. Partial support from the NSF, through grant ECCS-1230788 is also gratefully acknowledged.

References

[1] "Energy technology perspectives 2012 – pathways to a clean energy system," International Energy Agency, Tech. Rep. ETP2012, 2012. [Online]. Available: http://www.iea.org/etp/etp2012/

[2] G. Boyle, Ed., *Renewable Energy: Power for a Sustainable Future*, 2nd ed. Oxford University Press, 2004.

[3] US Energy Information Administration, "Annual energy outlooks 2010 with projections to 2035," U.S. Dept. of Energy, Tech. Rep. DOE/EIA-0383, 2010. [Online]. Available: http://www.eia.doe.gov/oiaf/aeo

[4] Zpryme Research & Consulting, "Power systems of the future: The case for energy storage, distributed generation, and microgrids," IEEE Smart Grid, Tech. Rep., Nov. 2012.

[5] P. Varaiya, F. Wu, and J. Bialek, "Smart operation of smart grid: Risk-limiting dispatch," *Proc. of the IEEE*, vol. 99, no. 1, pp. 40 –57, Jan. 2011.

[6] P. Kundur et al., "Definition and classification of power system stability IEEE/CIGRE joint task force on stability terms and definitions," *IEEE Trans. on Power Sys.*, vol. 19, no. 3, pp. 1387 – 1401, Aug. 2004.

[7] A. E. Motter, S. A. Myers, M. Anghel, and T. Nishikawa, "Spontaneous synchrony in power-grid networks," *Nature Physics*, vol. 9, no. 3, pp. 191–197, Feb. 2013.

[8] P. Varaiya, F. Wu, and R.-L. Chen, "Direct methods for transient stability analysis of power systems: Recent results," *Proc. of the IEEE*, vol. 73, no. 12, pp. 1703 – 1715, Dec. 1985.

[9] H.-D. Chiang, *Direct Methods for Stability Analysis of Electric Power Systems: Theoretical Foundation, BCU Methodologies, and Applications*. Wiley, 2011.

[10] L. Freris and D. Infield, *Renewable energy in power systems*. Chichester, U.K.: John Wiley and Sons, 2008.

[11] J. G. Slootweg and W. L. Kling, *Impacts of Wind Power on Power System Dynamics*. John Wiley and Sons, Ltd, 2005, pp. 629–651.

[12] R. Teodorescu, M. Liserre, and P. Rodriguez, *Grid Converters for Photovoltaic and Wind Power Systems*. Hoboken, NJ: John Wiley and Sons, 2010.

[13] F. Dörfler, M. Chertkov, and F. Bullo, "Synchronization in complex oscillator networks and smart grids," *Proc. of the Nat'l Academy of Sci.*, vol. 110, no. 6, pp. 2005–2010, 2013.

[14] A. R. Bergen and D. Hill, "A structure preserving model for power system stability analysis," *IEEE Trans. on Power Apparatus and Sys.*, vol. PAS-100, no. 1, pp. 25–35, 1981.

[15] E. Mallada and A. Tang, "Improving damping of power networks: Power scheduling and impedance adaptation," in *Proc. of the* 50^{th} *IEEE Conf. on Dec. and Ctrl.*, Orlando, FL, 2011, pp. 7729 – 7734.

[16] R. Robinett and D. Wilson, "Transient stability and control of renewable generators based on Hamiltonian surface shaping and power flow control: Part i-theory," in *Proc. of the IEEE Int'l Conf. on Control Applications*, 2010, pp. 2196–2202.

[17] J. Ekanayake, L. Holdsworth, X. G. Wu, and N. Jenkins, "Dynamic modeling of doubly fed induction generator wind turbines," *IEEE Trans. on Power Sys.*, vol. 18, no. 2, pp. 803–809, 2003.

[18] K. Elkington, J. G. Slootweg, M. Ghandhari, and W. L. Kling, *Reduced-Order Modelling of Wind Turbines*. John Wiley and Sons, Ltd, 2012, pp. 821–847.

[19] B. Lesieutre, P. Sauer, and M. A. Pai, "Development and comparative study of induction machine based dynamic P, Q load models," *IEEE Trans. on Power Sys.*, vol. 10, no. 1, pp. 182–191, 1995.

[20] B. Bamieh and D. Gayme, "The price of synchrony: Resistive losses due to phase synchronization in power networks," in *Proc. of the American Ctrl. Conf.*, June 2013, pp. 5815 – 5820.

[21] J. W. Simpson-Porco, F. Dörfler, and F. Bullo, "Droop-controlled inverters are Kuramoto oscillators," in *Proc. of the* 3^{rd} *IFAC Workshop on Distributed Estimation and Ctrl. in Networked Sys.*, Santa Barbara, CA, 2012, pp. 264–269.

[22] E. Sjödin, B. Bamieh, and D. Gayme, "The price of synchrony: Evaluating the resistive losses in synchronizing power networks," *Preprint*, 2014.

[23] A. Ghosh, S. Boyd, and A. Saberi, "Minimizing effective resistance of a graph," *SIAM Rev.*, vol. 50, no. 1, pp. 37–66, Feb. 1988.

[24] A. von Meier, *Electric Power Systems: A Conceptual Introduction*, E. Desurvire, Ed. Hoboken, NJ: John Wiley and Sons Inc., 2006.

[25] U. Miekkala, "Graph properties for splitting with grounded Laplacian matrices," *BIT Numerical Math.*, vol. 33, no. 3, pp. 485–495, 1993.

[26] E. Sjödin, "The price of synchrony: Evaluating transient power losses in renewable energy integrated power networks," 2013, MSc. Thesis, KTH, Automatic Control. [Online]. Available: http://urn.kb.se/resolve?urn=urn:nbn:se:kth:diva-133579

[27] M. Siami and N. Motee, "Fundamental limits on robustness measures in networks of interconnected systems," in *Proc. of the* 52^{nd} *IEEE Conf. on Dec. and Ctrl.*, Florence, Italy, 2013.